Phosphoinositide Turnover Imaging Linked to Muscarinic Cholinergic Receptor in the Central Nervous System by Positron Emission Tomography

Yoshio Imahori, Ryou Fujii, Satoshi Ueda, Yoshio Ohmori, Kazuo Wakita and Keigo Matsumoto

Department of Neurosurgery, Kyoto Prefectural University of Medicine, Kyoto, Japan; Nishijin Hospital, Kyoto, Japan

Receptor-mediated membrane processing plays an essential role in neural function in the synapses. In such neurotransmission process, the phosphoinositide (PI) response, an effector in the production of second-messengers, can be used to assess in vivo signal transduction. Using in vivo autoradiography and positron emission tomography (PET), we attempted to visualize the PI response to muscarinic cholinergic receptor (mAChR)-stimulation in rats and monkeys, which were administered 1,2-[^{11}C]diacylglycerol (DAG) intravenously. Enhancement of 1,2-[^{11}C]DAG incorporation was observed in the rat ipsilateral hippocampus and cortex in which mAChR-agonist was administered by local injection, but this was in contrast to spreading cortical depression in the ipsilateral cortex using KCl. In monkey PET studies, dynamic brain scanning revealed increase in activity over time for about 15 min after a bolus injection of 1,2-[^{11}C]DAG in an awake state. The activity then remained at a constant level. This finding documented the theoretical "membrane-trapping" mechanism. The systemic mAChR-stimulation accelerated incorporation in the cerebral cortices of the same monkey brain. Radioactivity uptake did not differ significantly between the mAChR-stimulated and nonstimulated early scan images. This suggested that cerebral blood flow does not greatly affect DAG incorporation. In sequential membrane processes of PI turnover, diacylglycerol kinase rapidly metabolizes DAG, included in PI turnover. In conclusion 1,2-[^{11}C]DAG incorporation was limited by receptor-mediated PI turnover, which can represent real synaptic transmission in neural networks.

J Nucl Med 1993; 34:1543–1551

The specific visualization of a neurotransmitter-receptor has been a challenge for many investigators studying the central nervous system (CNS) by positron emission tomography (PET) (*1–3*). However, not all receptors exert a direct effect on neurotransmission in the postsynaptic membrane. Biochemical reaction cascades can be induced by low molecular weight messenger substances following the binding of a neurotransmitter. Intracellular reaction cascades can reflect real synaptic transmission. Among these intracellular reaction cascades phosphoinositide (PI) turnover has been studied intensively (*4,5*). However, no assessments of this system have been attempted using in vivo measurement. Our previous studies suggest that the signal transduction system of PI turnover permits neurotransmission activity in synapses to be assessed (*6,7*). From this viewpoint we focused on PI turnover as a biochemical basis for the purpose of the imaging for activated neural networks. PI turnover possesses a dual system giving rise to elevation of intracellular Ca^{2+} by inositol trisphosphate (IP_3) (*8,9*) and the activation of Ca^{2+}-dependent protein phosphorylation by protein kinase C (PKC) with *sn*-1,2-diacylglycerol (DAG) (*10–12*). The latter component is usable as a tracer for assessing PI turnover. We previously found that uptake mechanism in a rat cerebral cortex that was administered with 1,2-[^{11}C]DAG was rapidly metabolized into phosphatidic acid (PA), phosphatidylinositol (PI), phosphatidylinositol-4-monophosphate (PIP), and phosphatidylinositol-4,5-bisphosphate (PIP_2), whereas radioactive phosphatidylcholine (PC) and phosphatidylethanolamine (PE) did not appear after 20 min (*7*). The *sn*-stereoisomer of 1,2-[^{11}C]DAG, administered even in a racemic mixture, can serve as a specific extrinsic tracer along with the PI regenerative pathway of DAG kinase, phosphatidylinositol 4-kinase (PI 4-kinase) and phosphatidylinositol 4-phosphate kinase (PIP 5-kinase), via CDP-DAG and is incorporated into the cerebral phosphoinositides. We synthesized ^{11}C-labeled *rac*-1,2-DAG by the ketene method (*13–16*). Diacylglycerols, which have a short-chained substituent with 1- or 2-butyryl residue, can be more suitable for attenuation of excessive lipophilicity, which is undesirable because of an increase in nonspecific tissue uptake of the tracers (*6*). We reported that the phosphorylated properties of short-chained diacylglycerols are equivalent to those of the native diacylglycerols in the PI regenerative pathway (*7*).

Of the CNS receptors coupled to PI turnover (*4,5,17*),

Received Aug. 19, 1992; revision accepted Apr. 1, 1993.

For correspondence and reprints contact: Yoshio Imahori, MD, PhD, Dept. of Neurosurgery, Kyoto Prefectural University of Medicine, Kawaramachi-Hirokouji, Kamigyo 602, Kyoto, Japan.

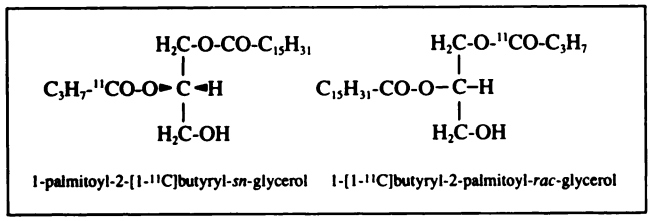

FIGURE 1. Chemical structures of ^{11}C-labeled diglyceride probes.

much detailed information has been obtained for muscarinic cholinergic receptors (mAChR) (*18–20*), which is found in high density in the neocortex (*21*). The incorporation of *rac*-1,2-[^{11}C]DAG is enhanced by systemic mAChR-stimulation (*7*). This finding suggests that *rac*-1,2-[^{11}C]DAG incorporation is related to receptor-mediated PI turnover in rat brain. We confirmed this by the local effect of mAChR-innervation on incorporation of *rac*-1,2-[^{11}C]DAG using the stereotactic microinjection into rat unilateral hippocampus. The effect of voltage-dependent neuronal activation that induces a spreading cortical depression (*22*) also was investigated. This model seemed suitable as a control because stimulus is not involved in receptor-mediated signal transduction.

This article also reports PET images of PI turnover in the conscious monkey, to verify whether brain incorporation of *rac*-1,2-[^{11}C]DAG is due to the membrane-trapping mechanism and documents time-activity curves in PET studies in the presence of mAChR-agonists, that is, the "PI response".

MATERIALS AND METHODS

1,2-[^{11}C]DAG Synthesis by Ketene Method

Carbon-11-labeled carbon dioxide was produced by the ^{14}N(p, α)^{11}C reaction using a cyclotron (The Japan Steel Works, model BC1710) and an automated synthesis system for producing [^{11}C]ethylketene (The Japan Steel Works, ARIS-C8). L-α-palmitoyl-2-[1-^{11}C]butyryl-*sn*-glycero-3-phosphorylcholine was obtained from L-α-palmitoyl-lysophosphatidylcholine by the [^{11}C]ethylketene reaction (*6,7*). The phosphorylcholine moiety was removed with phospholipase C (PLC; 5 units, Type 3 from *Bacillus cereus*) (*23,24*). Thereafter, 1-palmitoyl-2-[1-^{11}C]butyryl-*sn*-glycerol was obtained in the ether phase (*6,7*). To synthesize racemic ^{11}C-labeled DAG, [^{11}C]ethylketene was reacted in 300 μl of pyridine containing 1 μmol of 2-palmitoylglycerol and 0.5 μmol of dimethylaminopyridine at room temperature for 5 min. Unreacted [^{11}C]ethylketene, the ketene dimer and pyridine were completely removed by evaporation to yield 1-[1-^{11}C]butyryl-2-palmitoyl-*rac*-glycerol (*7*). These ^{11}C-labeled diglyceride probes (Fig. 1) were separated by HPLC (*7*).

Biodistribution of *rac*-1,2-[^{11}C]DAG under Conditions with Carrier DAG in Rat Brain

Tracer distribution in rats (male Wistar, each weighing 250–270 g) was measured by the following procedure. A dose of 3 mCi of [^{11}C]DAG dissolved in 0.4 ml saline containing 0.1% bovine serum albumin and 0.5% DMSO was injected into a conscious group with 5 μmol/kg of carrier-DAG (dipalmitoyl) (n = 4), a conscious group with 50 μmol/kg of carrier-DAG (dipalmitoyl) (n = 4), and into the control group (n = 4). Tracer was administered through the tail vein under transient anesthesia induced by halothane (1%–1.5%) in room air. Diacylglycerol loading was performed by intravenous injection of carrier-DAG at each concentration 3 min prior to intravenous injection of [^{11}C]DAG. An intravenous bolus injection of [^{11}C]DAG was given, and 30 min later, rats were killed by decapitation. The cerebral cortex (the cortical mantle) and cerebellum were rapidly removed and the radioactivity was measured using a gamma counter and the sample was weighed. Regional activity was calculated as %dose/g; (count/g tissue) × (1/total injected count) × 100%, and the regional incorporation was expressed as the brain/blood ratio. Data obtained from quadruplicate experiments are presented as average ± s.d.

Biodistribution of *rac*-1,2-[^{11}C]DAG Under Systemic mAChR-Stimulation and Spreading Cortical Depression in Rat Brain

General systemic mAChR-stimulation using arecoline has been reported (*7*). Tracer distribution in rats (male Wistar, each weighing 300–310 g) was measured by injecting a dose of 3 mCi of [^{11}C]DAG dissolved in 0.4 ml saline into rats in the conscious group with 5 μmol/kg of arecoline (n = 4), and in the control group (n = 4).

Spreading cortical depression was studied by means of subdural KCl injection (*22*). Tracer distribution in rats (male Wistar, each weighing 300–310 g) was measured by injecting a dose of 3 mCi of [^{11}C]DAG dissolved in 0.4 ml saline into rats in the conscious group with 3 *M* of KCl (n = 4), and in the sham-operated group using saline (n = 4).

Tracer was administered through the tail vein under transiently anesthetized conditions induced by halothane (1%–1.5%) in room air. An intravenous bolus injection of [^{11}C]DAG was given, and 30 min later the rats were killed by decapitation. The cerebral cortex and cerebellum were rapidly removed and the radioactivity was measured using a gamma counter and the sample weighed. Regional activity was calculated as %dose/g; (count/g tissue) × (1/total injected count) × 100%, and regional incorporation was expressed as the brain-to-blood ratio. Data obtained in quadruplicate experiments are presented as average ± s.d.

Local Microinjection of mAChR Agonist to Rat Brain

Wistar rats weighing 300 g were anesthetized with sodium pentobarbital (23 mg/kg) by intraperitoneal injection, and placed in a stereotactic frame. When the rats recovered from anesthesia, 1 mCi of *sn*-1,2-[^{11}C]DAG was administered intravenously followed immediately by a stereotactic local injection over a 5-min period of 5 μl of carbachol in 0.9% NaCl (2 m*M*, pH 7.4) using a Hamilton Microsyringe. Coordinates were determined using a rat-brain atlas (G. Paxinos and C. Watson, 1986) to locate the needle tip 2.0 mm laterally, 3.0 mm posteriorly and 3.0 mm in depth from the bregma. The rat was killed 30 min after the injection of *sn*-1,2-[^{11}C]DAG. The brain was rapidly removed and frozen in powdered dry ice. Autoradiographs were reconstructed from adjacent brain sections (40 μm thick) with the Fuji Computed Radiography System (FCR). The same stereotactic procedures were performed in the ^{18}F-labeled 2-fluoro-2-deoxyglucose ([^{18}F]FDG) study. Fluorine-18-FDG imaging was performed by the ordinary procedure of Sokoloff (*25*).

Anesthesia for Monkey PET Scanning

Qualitative images of brain radioactivity accumulation were obtained from male monkeys (*Macaca fuscata*) weighing 8–10 kg (n = 2) using PET. The experimental protocol involved a ket-

TABLE 1
Effect on Incorporation of 1,2-[^{11}C]DAG with Carrier-DAG (Dipalmitoylglycerol) and mAChR-agonist (Arecoline) by Systemic Administration

	(A)			(B)	
	Control mean ± s.d.	DAG (+) 5 μmol/kg of DP mean ± s.d.	DAG (++) 50 μmol/kg of DP mean ± s.d.	Control The systemic cholinergic blockage (+) mean ± s.d.	Arecoline (+) mean ± s.d.
Cerebral cortex/blood	0.69 ± 0.06	0.87 ± 0.11*	0.80 ± 0.11†	0.82 ± 0.06	0.98 ± 0.06*
Cerebellum/blood	0.66 ± 0.09	0.75 ± 0.05†	0.70 ± 0.08‡	0.68 ± 0.06	0.88 ± 0.06*

*$0.05 < p < 0.1$.
†$p < 0.25$.
‡Not significant.
The effect on 1-[1-^{11}C]butyryl-2-palmitoyl-*rac*-glycerol incorporation was examined by administration of nonradioactive dipalmitoylglycerol (DP) IV injection and arecoline IP injection. (A) For comparison between the control group (n = 4) and carrier DAG-added groups (n = 4) by t-test. (B) For comparison between the control group (n = 4) and mAChR-stimulated group (n = 4) by t-test. The total injection dose of 1-[1-^{11}C]butyryl-2-palmitoyl-*rac*-glycerol was 3 mCi per rat. Rats were killed 30 min after injection. Regional incorporation was expressed as the brain-to-blood ratio. Data presents an average ± s.d. (n = 4).

amine/pentobarbital preanesthetic, followed by intubation with a cuffed endotracheal tube and mechanical ventilation. Lidocaine was used as the local anesthesia prior to cut-down. Pancronium bromide (0.06 mg/kg/hr; intravenously) was used for immobilization during scan. A respirator was adjusted to maintain arterial gases within normal physiological range with continuous monitoring of end-tidal CO_2; intermittent arterial blood was sampled at regular intervals throughout the scan to measure hematocrit, blood pH, $PaCO_2$, and PaO_2. Mean arterial blood pressure and rectal temperature also were monitored.

Monkey PET Imaging

PET scans were conducted with a tomograph based on the HEADTOME III design (Shimadzu Co., Japan). The in-plane resolution was 8.6 mm FWHM, while the axial resolution averaged 13.6 mm. Immobilized monkeys were positioned on a tray, and their heads were strapped to the tray with adhesive tape. The first PET scans (n = 2) were performed in a resting-awake-state and the second scans (n = 1) were performed in a mAChR-stimulated state under controlled ventilation. In both PET scans, systemic cholinergic blockage (*7,26*) was achieved using butylscopolamine bromide (6.6 mg/kg; s.c.). A dose of 1-[1-^{11}C]butyryl-2-palmitoyl-*rac*-glycerol (3 mCi/10 kg body weight) was injected intravenously. A rapid infusion method was used, in which a 5-ml intravenous-injection of tracer was performed for 20 sec. The PET camera was used to continuously collect data 15 times with 2-min intervals, and the dynamics of ^{11}C radioactivity in the brain was monitored. Simultaneously, arterial blood was sampled and the ^{11}C radioactivity was sequentially measured. The initiation time, T = 0, was set when the whole-brain activity reached a value greater than that of the background activity in PET camera. We set the PET counting area with 49 pixels on each region of interest (ROI; 7 × 7 pixels). The variation of each count for a single counting area is settled at less than 18% s.d.

Blood Sampling and Analysis

A sequence of arterial blood samples (500 μl) was collected. The first five samples were obtained at 10-sec intervals. The remainder samples were obtained at gradually longer intervals (0.5 min–5 min), making a total of 17 samples within a period of 30 min. The degradation of 1-[1-^{11}C]butyryl-2-palmitoyl-*rac*-glycerol was studied in monkey serum. Serum samples were then applied to silica on TLC plates, in which 1,2-[^{11}C]DAG was separated from all polarized components by means of a solvent system consisting of chloroform/methanol/water: 65/25/4 (v/v). The plates (length, 75 mm) were developed in one dimension, then divided into two fractions that were counted (1,2-DAG was located at the top and all other polarized components at the bottom).

Use of mAChR-Stimulation in PET Study in Monkey Brain

Arecoline was administered under systemic cholinergic blockage using butylscopolamine bromide to study mAChR-stimulation (n = 1). A male monkey weighing 10 kg was given saline with butylscopolamine bromide (6.6 mg/kg; s.c.) 20 min prior to an intraperitoneal injection of arecoline (13 mg/kg). Five minutes after arecoline injection, 3 mCi of 1-[1-^{11}C]butyryl-2-palmitoyl-*rac*-glycerol was injected intravenously through the femoral vein. The PET camera was used to continuously collect data for 15 times at 2 min intervals and the dynamics of brain ^{11}C radioactivity was monitored. Arterial blood was sampled simultaneously and ^{11}C radioactivity measured sequentially.

RESULTS

Effect on Incorporation of *rac*-1,2-[^{11}C]DAG with Carrier-DAG

The biodistribution study, which involved addition of 5 μmol/kg of carrier DAG, revealed a 25% increase of [^{11}C]DAG incorporation in the carrier-DAG-treated group when compared with the control ($0.05 < p < 0.1$) (Table 1). When 50 μmol/kg of carrier DAG was added, [^{11}C]DAG incorporation increased by 16% when compared with controls ($p < 0.25$). The results suggest that the DAG incorporation mechanism does not depend on receptor-ligand interaction.

Effect on Incorporation of *rac*-1,2-[^{11}C]DAG by mAChR-Stimulation

As shown in Table 1, mAChR-stimulation induced by systemic administration of arecoline caused a rise in DAG incorporation (20%–30%) in the cortex and cerebellum relative to controls ($0.05 < p < 0.1$).

TABLE 2
Effect on Incorporation of 1,2-[^{11}C]DAG by the Spreading Cortical Depression

	Sham operation Local injection of 5 μl of saline		KCl (+) Local injection of 5 μl of 3 *M* KCl	
	Contralateral cortex control mean ± s.d.	Ipsilateral cortex 0.9% NaCl (+) mean ± s.d.	Contralateral cortex control mean ± s.d.	Ipsilateral cortex 3 *M* KCl (+) mean ± s.d.
Cerebral cortex/blood	0.76 ± 0.09	0.77 ± 0.07	0.70 ± 0.05	0.66 ± 0.07*
Cerebellum/blood	0.70 ± 0.08	—	0.65 ± 0.02	—

*$0.05 < p < 0.1$.

The effect of K^+ on 1-[1-^{11}C]butyryl-2-palmitoyl-*rac*-glycerol incorporation was examined by administration of 3 *M* KCl to the subdural space overlying the left parietal cortex. The sham operation was used with 0.9% NaCl by the same manner. The total injection dose of 1-[1-^{11}C]butyryl-2-palmitoyl-*rac*-glycerol was 3 mCi per rat. The rats were killed 30 min after injection. Regional incorporation was expressed as the brain-to-blood ratio. For comparison between the sham operation group (n = 4) and 3 *M* of KCl-added group (n = 4) by t-test. Data presents an average ± s.d.

Effect on Incorporation of *rac*-1,2-[^{11}C]DAG by Spreading Cortical Depression

Spreading cortical depression induced by subdural injection of KCl to the ipsilateral hemisphere in the cortex decreased DAG incorporation by 15% (0.66 ± 0.07) compared with the sham-operated group (0.77 ± 0.07), as shown in Table 2. Incorporation was also attenuated in the contralateral cortex in the spreading cortical depression group.

Local Stimulation of mAChR-Agonist in Rat Brain

Regions with high muscarinic cholinoceptive neurons, such as in the cerebral cortex (Cx), entorhinal cortex (Ec), hippocampus (Hc), and amygdaloid nucleus (Ag), corresponded with those showing high-grade incorporation of *sn*-1,2-[^{11}C]DAG (*6*). Typical autoradiographic maps of 1,2-[^{11}C]DAG uptake sites in the brain of the conscious rat showed a column-like pattern in the cerebral cortex (Cx) that was vertical to the cortical laminae. The lateral geniculate body (LG) was demarcated (on right). The caudate putamen (CPu) was visible but the globus pallidus (Gp) and thalamus (Th) were less visible (Fig. 2). We studied regions with high cholinoceptive neurons by microinjection using carbachol. As shown in Figure 3 (left), carbachol enhanced accumulation of *sn*-1,2-[^{11}C]DAG in the right hippocampus and cerebral cortex. Microinjection of 5 μl of the carbachol (2 m*M*) to the right hippocampus resulted in spread into the lateral ventricle and subarachnoid space near the puncture point, inducing activation in the ipsilateral cortical neurons. In the [^{18}F]FDG study, the high glucose metabolism was observed in an area with cholinergic stimulation in Figure 3 (right).

Monkey PET Imaging and the Mathematical Model

Dynamic scanning of monkeys using PET revealed increase in activity over time for about 15 min after bolus injection of 1,2-[^{11}C]DAG. Activity in the brain (Fig. 4A) remained constant in time-activity curves (*Pre-stimulation* in Fig. 4B). This finding supports the "membrane-trapping" mechanism previously presented (*7*), which allows the DAG metabolic rate to be quantified as described below. Sequential second scans conducted during mAChR-stimulation revealed the same pattern with an exaggerated tendency (*Post-stimulation* in Fig. 4B).

The C^*_{br} indicates the ^{11}C-phosphoinositides for the entire amount of incorporated membrane phosphoinositides. The mathematical model for data analysis can be described by the following equation:

$$[k^* \text{ (ml s}^{-1}\text{g}^{-1}) \times 10^4] = C^*_{br}(T) \Big/ \int_0^T C^*_{pl}\, dt.$$

This equation has been defined as the incorporation constant (*26*). Radioactivity in each brain region (C^*_{br}), which was the sum of the membrane phosphoinositide compartments ($C^*_{br,i}$), was determined. Since $C^*_{br,i}$ represents phos-

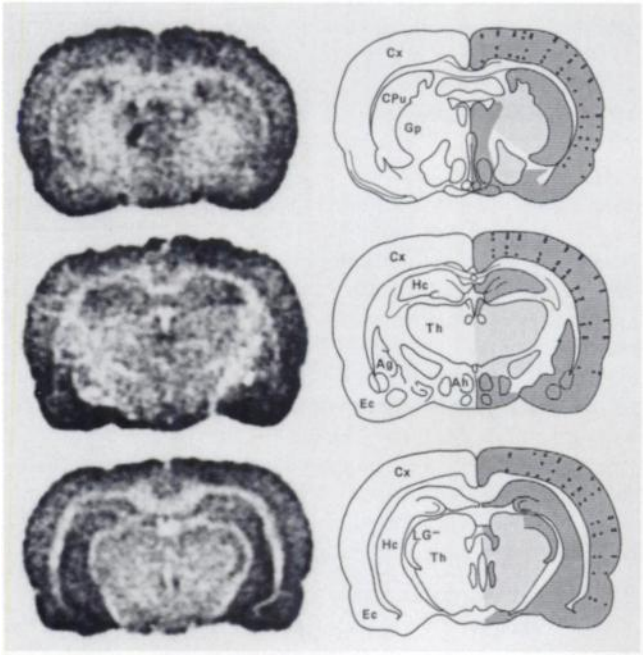

FIGURE 2. Typical autoradiographic maps of 1-[1-^{11}C]butyryl-2-palmitoyl-*rac*-glycerol incorporation sites in the brain of the conscious rat. The cerebral cortex (Cx), hippocampus (Hc), amygdaloid nucleus (Ag), anterior hypothalamus (Ah), entorhinal cortex (Ec), lateral geniculate body (LG), caudate putamen (CPu), globus pallidus (Gp), and thalamus (Th).

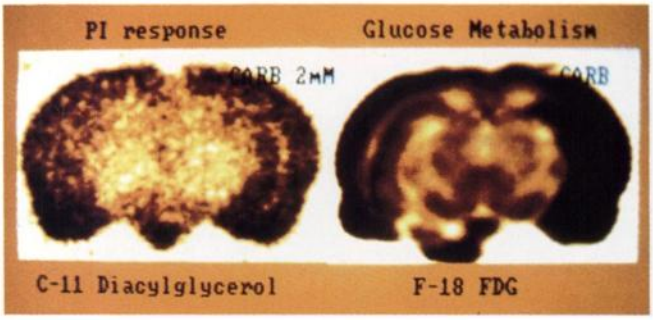

FIGURE 3. 1-palmitoyl-2-[1-^{11}C]butyryl-*sn*-glycerol (1.5 mCi) was administered intravenously, immediately followed by a stereotactic local injection of 5 μl of carbachol solution (2 m*M*). The stimulated side was on the right in the rat brain. The autoradiograph was from an adjacent section of 40 μm thickness (on the plane −4.8 mm posteriorly from the Bregma) and was reconstructed with the FCR System. The fluorine-18-labeled 2-fluoro-2-deoxyglucose (^{18}F FDG) study was performed under the same conditions. This autoradiograph was on the plane −5.6 mm posteriorly from the Bregma.

phoinositide components on the same system, we regarded C^*_{br} to be equal to $\Sigma C^*_{br,i}$ based on the membrane-trapping mechanism. The C^*_{br} was divided by plasma nonmetabolized 1,2-DAG radioactivity (C^*_{pl}), integrated over the duration (T) of the experiment. This calculation normalizes brain radioactivity to exposure under the plasma curve and results in an estimate of the unidirectional incorporation rate constant ([k* (ml $s^{-1}g^{-1}$) × 10^4]). From time-activity curves, we defined integration time (T) as 15 min (900 sec).

Changes in DAG-Incorporation Rate by mAChR-Stimulation in DAG-PET Study in a Monkey Brain

Figure 5 shows PET images in early (2 min) and delayed (16 min) scans representing time-sequential dynamic PET in pre- and poststimulation with arecoline. Systemic mAChR-stimulation accelerated incorporation in cerebral cortices of the monkey brain in the delayed scan image (D). However, radioactivity uptake did not differ significantly between mAChR-stimulated (C) and nonstimulated (A) early scan images.

As shown in Table 3, resting k* constant was higher in the occipital region than in other brain regions. The k* constant in white matter was about 85% of values in the occipital region. The percentage should be regarded as overestimation due to holding the cortices. When stimulated with arecoline, the k* constant increased by 20% in the occipital, temporal and frontal cortices, while there was no effect on the temporal muscle. The increase is similar to that obtained in the rat. The k* constant in the stimulated state was higher in the occipital (retrocalcarine and lateral calcarine) region (*27*) than in any other regions (Fig. 4A and 5).

Blood Sampling and Correction of Time-Activity Curve

Degradation of 1,2-[^{11}C]DAG was studied in monkey serum. Figure 6 shows a typical corrected time-activity curve for pre-stimulation with mAChR. Figure 7 shows nonpolarized fraction on TLC from time-sequential serum

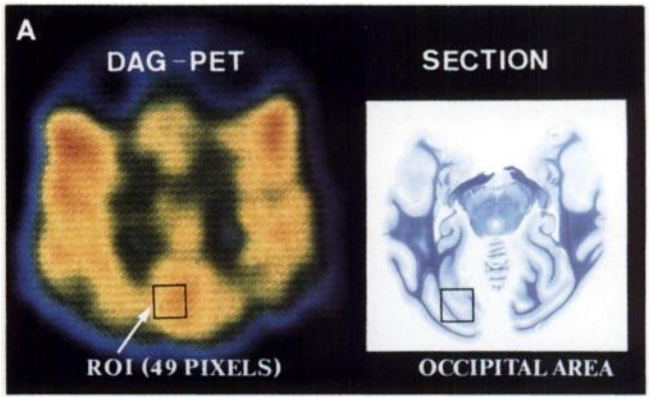

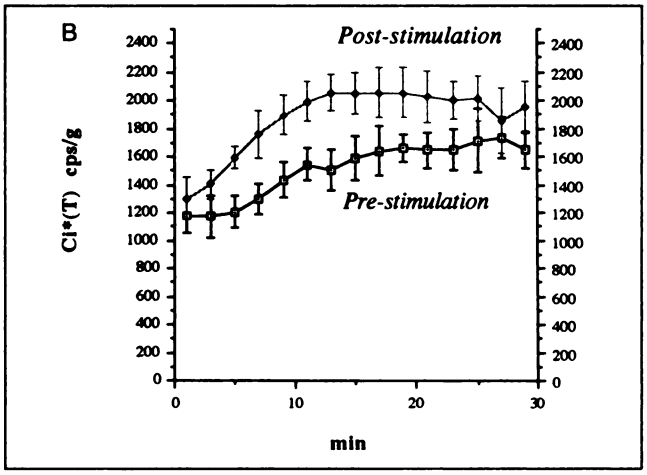

FIGURE 4. (A) DAG-PET image in equilibrium state at 16 min under mAChR-stimulation in a male monkey (*Macaca fuscata*) weighing 10 kg. A square area indicates the ROI in the occipital area involved with high DAG accumulation by cholinergic innervation. Section stained by Klüver-Barrera method showing same level of axial PET scan. Visual cortices account for a large part of the occipital area. (B) Time-activity curves obtained in monkey brain (a typical profile) showing "membrane-trapping" profile. The in-plane resolution was 8.6 mm FWHM, while the axial resolution averaged was 13.6 mm. First PET scans performed in resting state (*pre-stimulation*) and second scans performed in mAChR-stimulated state (*post-stimulation*). Serial scans made at 3-hr intervals. In both PET scans systemic cholinergic blockage performed using butylscopolamine bromide.

samples. Degradation of 1-[1-^{11}C]butyryl-2-palmitoyl-*rac*-glycerol occurred rapidly in serum. No difference in the degradation rate occurred between the resting and mAChR-stimulated conditions. Almost all 1,2-[^{11}C]DAG disappeared within 15 min. Practically, the 1,2-[^{11}C]DAG incorporation can be seen within 15 min in sequential PET scans. The ^{11}C-labeled metabolized component in serum has to be deduced from total serum activity, representing corrected input function. Correction was calculated based on Figure 7.

DISCUSSION

In this study, we examined use of diglyceride probes for imaging PI turnover in vivo. For such a study, a technique was needed for measuring PI turnover that would not be overstated due to use of Li^+ blockage (*8*). Previously we demonstrated direct incorporation of radiolabeled DAG

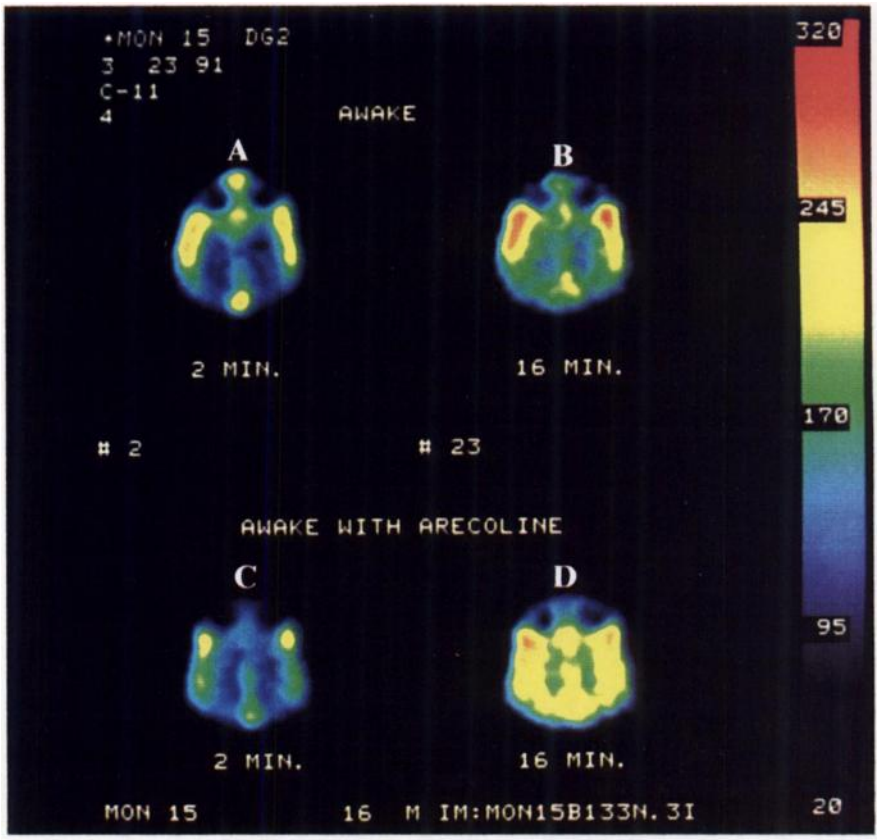

FIGURE 5. DAG-PET images in resting state of monkey brain. (A) early scan image at 2 min; (B) delayed scan image at 16 min) and in mAChR-stimulated state of same brain; (C) early scan image at 2 min; and (D) delayed scan image at 16 min).

into cerebral phosphoinositide along with PI recycling, without Li^+ blockage. In the brain, characterized by highly efficient synaptic neurotransmission, DAG level usually remains low to prepare for signalling. DAG is thus a more appropriate precursor in the central nervous system (CNS). By contrast, DAG level is high in proliferating cells, suggesting a continuous release of proliferation signals (*28*). In this study, we examined in detail uptake of diglyceride probes in rats and monkeys after administration of cholinergic drugs systemically and intracerebrally and during KCl-induced spreading cortical depression.

TABLE 3
Changes in Intrasubject DAG-Incorporation Rate Between Pre- and Post-mAChR-Stimulation in DAG-PET Study in Monkey Brain

	Control (Resting state) mean ± s.d.	mAChR-stimulated with arecoline mean ± s.d.	% increase mAChR-stimulated/Control
	Incorporation constant; [k^* (ml $s^{-1}g^{-1}$) × 10^4]		
Cerebral cortices			
Frontal cortex (front-orbital)	4.54 ± 0.36	5.57 ± 0.42*	123% ⇑
Temporal cortex	4.69 ± 0.37	5.56 ± 0.45*	119% ⇑
Occipital cortex (retro-calcarine)	5.00 ± 0.52	5.92 ± 0.40*	118% ⇑
White matter	4.19 ± 0.43	4.93 ± 0.45*	118% ⇑
Temporal muscle	6.46 ± 0.72	6.10 ± 0.41*	94% ⇓

*$p < 0.01$.

The effect of mAChR-stimulation on 1-[1-^{11}C]butyryl-2-palmitoyl-*rac*-glycerol incorporation was examined by dynamic PET studies. The mathematical model for data analysis was detailed in reference 26. Incorporation constant values are represented as [k^* (ml $s^{-1}g^{-1}$) × 10^4]. For comparison between the control group (in the first PET scan) and mAChR-stimulated groups (in the second PET scan) by t-test. The total injection dose was 3 mCi per monkey. PET data were collected from each region of interest (ROI; 7 × 7 pixels) within the variation of 18% s.d. of each pixel counts. Data presents an average ± s.d.

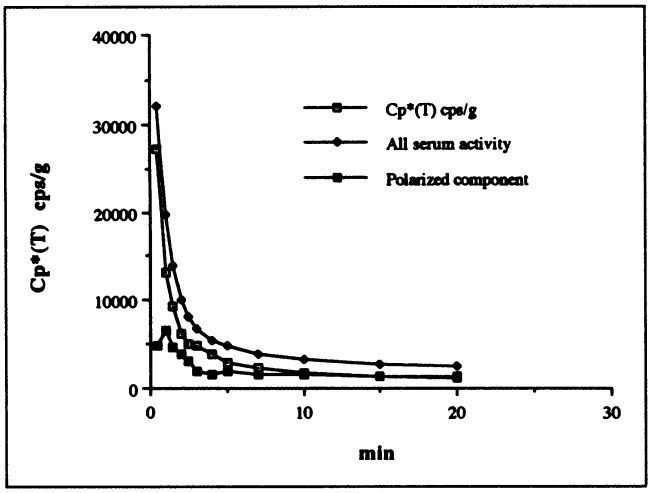

FIGURE 6. Typical input-function (Cp*(T); cps/g) of pre-mAChR-stimulation in monkey PET study. Correction of time-activity curve performed based on nonpolarized radioactive fractions on time-sequential TLC from serum.

Carbon-11-DAG Incorporation Represented as an Aspect of PI Turnover

In dilution experiments using a DAG carrier, 1,2-[^{11}C]-DAG incorporation was not attenuated; rather, the incorporation was elevated as shown in Table 1. This suggests that the receptor-binding mechanism to protein kinase C (PKC) does not serve as an important factor determining DAG incorporation. One explanation may be activation of 1,2-diacylglycerol kinase (DAG kinase) by an excess of DAG (*29*). Namely, excessive DAG carrier elevates DAG concentration in the cell membrane and activates PKC, inducing activated DAG kinase due to protein phosphorylation (*30,31*). The native DAG with an acyl residue of polyunsaturated free fatty acid such as arachidonate at the second position has high PKC-binding affinity, allowing more efficient activation of PKC (*17,32*). The ^{11}C-labeled DAG, however, has saturated acyl residues like palmitoyl, stearoyl and butyryl and its role as a PI-metabolic precursor is marked. We recently developed ^{11}C-labeled phorbol esters for use as PKC-imaging probes (*33*) but these compounds are not metabolized along with PI turnover.

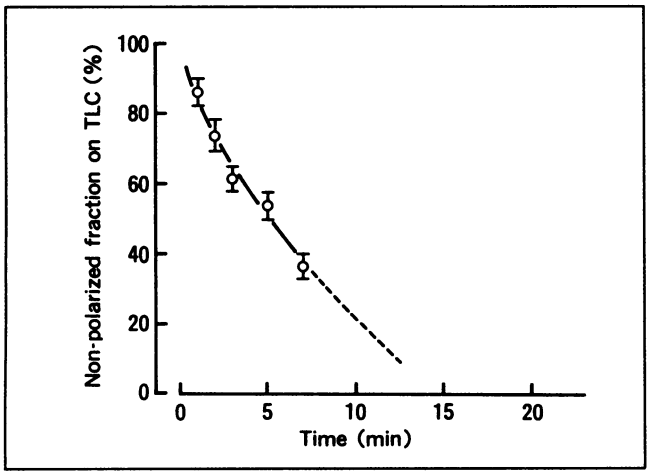

FIGURE 7. Percentage of nonpolarized fraction represents non-metabolized [^{11}C]DAG in serum based on time-sequential TLC studies. Correction of time-activity curve performed using this figure. Dotted curve drawn by projection.

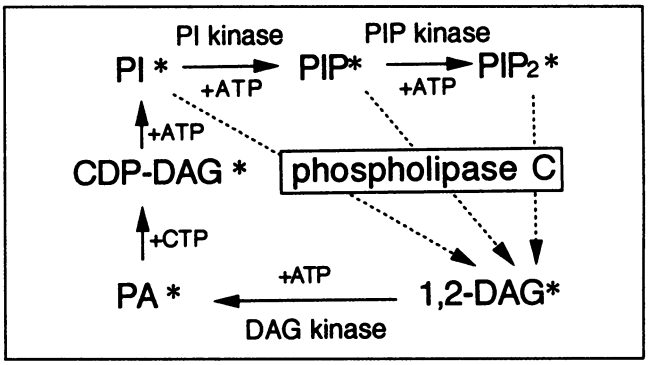

FIGURE 8. DAG kinase works as key enzyme in PI turnover. This should be regarded as integration process of PI recycling system. Asterisk (*) indicates ^{11}C-labeled component. Dotted arrows mean remobilization of ^{11}C-DAG. However, this seems to be a poor possibility.

DAG kinase is activated through translocation (*29,34*). The PA level in the CNS remains very low in normal brain tissue, as does DAG. This is due to regulation by DAG kinase, which catalyzes the following reaction:

$$1,2\text{-DAG} + \text{ATP} \Rightarrow \text{PA} + \text{ADP}.$$

In steady state, a DAG kinase-PA phosphatase conjugate regulates phospholipid metabolism. Our results indicate that this balance is shifted toward PA in nerve tissue (*7*). The study was designed to determine status of DAG recycling, including assessment of PKC activity. DAG incorporation represents an aspect of PI turnover. Imaging DAG incorporation seems to visualize activity of DAG kinase, a key enzyme in PI turnover. Phosphatidic acid, formed in the presence of this enzyme, is changed via CDP-DAG into PI in the presence of PI synthetase. Phosphatidylinositol is then converted into PIP by PI kinase. Phosphatidylinositol-4-phosphate is converted into PIP_2 by PIP 5-kinase (*5,8*). Through this sequential metabolic process, a phosphoinositide tracer pool is formed. We referred to this phenomenon as membrane trapping because the possibility of remobilization of ^{11}C-labeled phosphoinositide (PIPs), attenuated by the native membrane PIPs, seems to be very low (*7*). The tracer pool can be regarded as representing integration of phosphoinositide downstream from PA produced by DAG kinase, as summarized in Figure 8. Because its specificity for DAG kinase is extremely low in vitro (*35*), 1,3-[^{11}C]DAG is suitable for use in nonspecific uptake studies. Thus, 1,3-[^{11}C]DAG should be regarded as a nonspecific PI turnover tracer. However, in vivo studies reveal some polarized metabolites of 1,3-[^{11}C]DAG and their accumulation in rat brain (*6*).

Difference in the Effects between mAChR-Stimulation and Spreading Cortical Depression

Enhancement of 1,2-[^{11}C]DAG incorporation reflects characteristics of PI turnover in cholinoceptive neurons in rat hippocampus stimulated by locally injected mAChR-

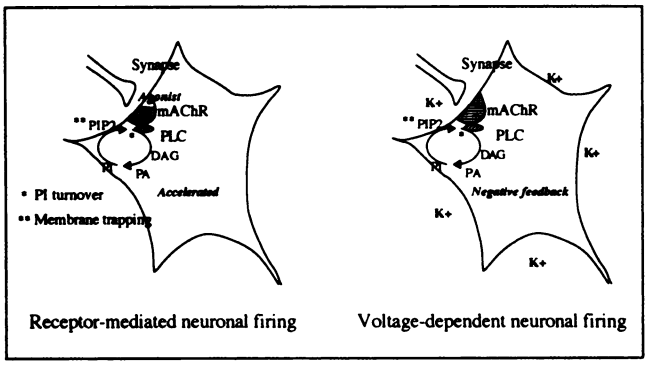

FIGURE 9. Effect on [^{11}C]DAG incorporation induced by receptor-mediated neuronal firing (*cholinergic innervation*) and voltage-dependent neuronal firing (*spreading cortical depression*).

agonist (Fig. 3). The [^{18}F]FDG study showed high glucose metabolism in an area of cholinergic stimulation by carbachol (Fig. 3), suggesting that accelerated 1,2-[^{11}C]DAG incorporation reflects synaptic events that need high glucose energy consumption. In addition, systemic mAChR-stimulation also prompted incorporation of [^{11}C]DAG in rat brain, however, effects of the voltage-dependent neuronal activation induced by spreading cortical depression (SCD) differed. PI turnover can be driven by phosphorylation by ATP (*8*). However, Table 2 shows that spreading cortical depression induced by KCl cannot accelerate 1,2-[^{11}C]DAG incorporation despite evidence of induced [^{18}F]FDG uptake (*22,25,* unpublished data). The 15% reduction in DAG incorporation (Table 2) may be due to specific negative-feedback under voltage-dependent neuronal firing. This also suggests that cerebral blood flow (CBF) does not greatly affect DAG incorporation, since it also should have been elevated. These findings strongly suggest that 1,2-[^{11}C]DAG incorporation is limited by receptor-linked membrane processing (Fig. 9).

Phosphoinositide Turnover Image in CNS by PET

Dynamic PET images demonstrate an incorporation profile in the brain and time-activity curves support the notion of a membrane-trapping mechanism. The k* constant was more than twice the incorporation rate for [^{14}C]arachidonate or [^{14}C]docosahexaenoate shown in the rat by DeGeorge et al. (*26*). Even when differences in the species of the experimental animals are considered, the higher incorporation rate for 1,2-[^{11}C]DAG can be interpreted as representing its specific incorporation into phosphoinositide alone. When stimulated with arecoline, the k* constant was about 20% higher than its resting value. This percentage of increase is similar to that previously obtained using rats (*7*). However, these conclusions were drawn from the single primate study in which the mAChR-agonist was administered. Although PET is the most reliable in vivo measurement tool now available, further studies are required to obtain intersubject information. When we compared early scan images (Fig. 5A and C), radioactivity uptake did not differ significantly between mAChR-stimulated and nonstimulated scan images. The result suggests that CBF does not greatly affect DAG incorporation.

A PET study of monkey brain in a resting condition revealed higher activity in the occipital region, including the visual field area (Fig. 5B and Fig. 4A). Stimulation with arecoline resulted in elevation in DAG incorporation in the whole brain, especially in the occipital cortex (Fig. 5D). Change in regional DAG incorporation due to systemic administration of a mAChR-agonist probably represents PI response to mAChR, producing regional specific brain mapping for mAChR-related signal transduction. As shown in Table 3, variation of 20% increase in k* constant following stimulation indicates that PET also allows measurement of PI response in vivo. If a more accurate mathematical model is developed, it will become possible to achieve postsynaptic signal transduction mapping of the human brain under physiological and pathological conditions with higher accuracy.

Postsynaptic Signal Generation Faithfully Mirrors Status of Neural Activity

The presynaptic terminal converts electrical into chemical signals. Transmembrane receptor systems, which activate a membrane-bound phospholipase C via the G protein, control postsynaptic signal generation. Under pathological conditions involving down-regulation or up-regulation of receptors, it is impossible to identify postsynaptic response by examining the number of receptors using conventional receptor-ligand assay. However, signal transduction imaging may allow quantification of postsynaptic responses. This approach in vivo can clarify response of neuronal receptors and may give a clue to elucidating new biological mechanisms of neural functions such as learning and memory. Abnormalities of the mAChR-related neurotransmission process have been thought to be an important factor in patients with dementia in Alzheimer's disease (*36,37*). However, it is not clear which process (the cholinergic innervation and mAChR-binding, or the intracellular reaction cascades that follow) is primarily responsible for the affected cortical functions. Since the disease involves dysfunctional synaptic transmission, activity of neurons in these patients can be clarified by examining the receptor-mediated PI turnover, making qualitative diagnosis of Alzheimer's disease and quantitative diagnosis of cholinergic innervation possible. Because radiolabeled DAG can be incorporated in proportion to PI turnover activity, synaptic transmission status may be evaluated in a neural system, excluding effect of glial proliferation. This property may be useful for evaluating neurotransmission damage in Alzheimer's disease or other degenerative conditions, ischemic brain disease and traumatic brain damage. Imaging of signal transduction in vivo will provide a much more powerful tool for use in neurobiological research.

ACKNOWLEDGMENT

Animal experiments and care followed the Guidelines for the Care and Use of Laboratory Animals established by The Animal Care Committee of Kyoto Prefectural University of Medicine. The authors thank Professor Kinya Kuriyama, MD, for advice on this manuscript; Dr. Hiroshi Tenjin, whose medical-technical expertise in anesthesia was invaluable; and Mr. Hitoshi Horii for his skillful technical assistance for PET. This work was supported in part by a Grant-in-Aid for Science Research (02454337) from the Ministry of Education Science and Culture of Japan.

REFERENCES

1. Comar D, Maziere M, Godot JM, et al. Visualization of ^{11}C-flunitrazepam displacement in the brain of the live baboon. *Nature* 1979;280:329–331.
2. Wagner, Jr, HN, Burns HD, Dannals RF, et al. Imaging dopamine receptors in the human brain by positron tomography. *Science* 1983;221:1264–1266.
3. Garnett ES, Firnau G, Nahmias C. Dopamine visualized in the basal ganglia of living man. *Nature* 1983;305:137–138.
4. Snider RM, Fisher SK, Agranoff BW. Inositide-linked second messengers in the central nervous system. In: Meltzer HY, ed. *Psychopharmacology: the third generation of progress.* New York: Raven Press; 1987:317–324.
5. Fisher SK, Heacock AM, Agranoff BW. Inositol lipids and signal transduction in the nervous system: An update. *J Neurochem* 1992;58:18–38.
6. Imahori Y, Fujii R, Ueda S, et al. No-carrier-added carbon-11-labeled *sn*-1,2-and *sn*-1,3-diacylglycerols by [^{11}C]propyl ketene method. *J Nucl Med* 1991;32:1622–1626.
7. Imahori Y, Fujii R, Ueda S, et al. Membrane trapping of carbon-11-labeled 1,2-diacylglycerol as a basic concept for assessing phosphatidylinositol turnover in neurotransmission process. *J Nucl Med* 1992;33:413–422.
8. Berridge MJ. Inositol trisphosphate and diacylglycerol as second messengers. *Biochem J* 1984;220:345–360.
9. Berridge MJ, Irvine RF. Inositol phosphates and cell signaling. *Nature* 1989;341:197–205.
10. Kikkawa U, Takai Y, Tanaka Y, Miyake R, Nishizuka Y. Protein kinase C as a possible receptor protein of tumor-promoting phorbol esters. *J Biol Chem* 1983;258:11442–11445.
11. Nishizuka Y. The role of protein kinase C in cell surface signal transduction and tumour promotion. *Nature* 1984;308:693–698.
12. Nishizuka Y. Studies and perspectives of protein kinase C. *Science* 1986; 233:305–312.
13. Imahori Y, Fujii R, Ido T, et al. Positron labeled phorbol ester: synthesis method for "non-carrier added" phorbol 13-[1-^{11}C]butyrate using ketene reaction. *J Labelled Compd Radiopharm* 1989;27:1025–1034.
14. Fujii R, Imahori Y, Ido T, et al. New synthesis method of [1-^{11}C]proryl keteneusing HCl/He gas mixture and the reactions on various alcohols. In: *Eighth international symposium on radiopharmaceutical chemistry,* West Sussex, England: Wiley. 1990;123–124.
15. Fujii R, Imahori Y, Ido T, et al. New synthesis system of (C-11)propyl ketene and its reactions with various alcohols. *J Labelled Compd Radiopharm* 1991;29:497–505.
16. Imahori Y, Fujii R, Ueda S. Incorrect naming of a carbon-11-labeled reagent [Letter]. *J Nucl Med* 1992;33:465–466.
17. Agranoff BW. Phosphoinositides. In: Siegel GJ, et al. ed. *Basic Neurochemistry: molecular, cellular, and medical aspects, fourth edition.* New York: Raven Press; 1989;333–347.
18. Durell J, Garland JT, Friedel RO. Acetylcholine action: biochemical aspects. *Science* 1969;165:862–866.
19. Soukup JF, Friedel RO, Schanberg SM. Cholinergic stimulation of polyphoshoinositide metabolism in brain in vivo. *Biochem Pharmacol* 1978;27: 1239–1243.
20. Janowsky A, Labarca R, Paul SM. Characterization of neurotransmitter receptor-mediated phosphatidylinositol hydrolysis in the rat hippocampus. *Life Sciences* 1984;35:1953–1961.
21. Emson PC, Lindvall O. Distribution of putative neurotransmitters in the neocortex. *Neuroscience* 1979;4:1–30.
22. Shinohara M, Rapoport S, Sokoloff L. Cerebral glucose utilization: local changes during and after recovery from spreading cortical depression. *Science* 1979;203:188–190.
23. Zwaal RFA, Roelofsen B, Comfurius P, Van Deenen LLM. Complete purification and some properties of phospholipase C from Bacillus cereus. *Biochim Biophys Acta* 1971;233:474–479.
24. Cabot MC, Jaken S. Structural and chemical specificity of diradylglycerols for protein kinase C activation. *Biochem Biophys Res Commun* 1984;125: 163–169.
25. Sokoloff L. Localization of functional activity in the central nervous system by measurement of glucose utilization with radioactive deoxyglucose. *J Cereb Blood Flow Metab* 1981;1:7–36.
26. DeGeorge JJ, Nariai T, Yamazaki S, Williams WM, Rapoport SI. Arecoline-stimulated brain incorporation of intravenously administrated fatty acids in unanesthetized rats. *J Neurochem* 1991;56:352–355.
27. Connolly CJ. *Experimental morphology of the primate brain.* Springfield, Illinois: Charles C. Thomas; 1950.
28. Fleischman LF, Chahwala SB, Cantley L. *Ras*-transformed cells: altered levels of phosphatidylinositol-4,5-bisphosphate and catabolites. *Science* 1986;231:407–410.
29. Besterman JM, Pollenz RS, Booker Jr EL, Cuatrecasas P. Diacylglycerol-induced translocation of diacylglycerol kinase: use of affinity-purified enzyme in a reconstitution system. *Proc Natl Acad Sci USA* 1986;83:9378–9382.
30. Kanoh H, Åkesson B. Properties of microsomal and soluble diacylglycerol kinase in rat liver. *Eur J Biochem* 1978;85:225–232.
31. Kanoh H, Yamada K, Sakane F. Diacylglycerol kinase: a key modulator of signal transduction? *Trends Biochem Sci* 1990;15:47–50.
32. Mori T, Takai Y, Yu B, et al. Specificity of the fatty acyl moieties of diacylglycerol for the activation of calcium-activated, phospholipid-dependent protein kinase. *J Biochem* 1982;91:427–431.
33. Ohmori Y, Imahori Y, Ueda S, et al. Protein kinase C imaging using carbon-11-labeled phorbol esters: 12-deoxyphorbol 13-isobutyrate-20-[1-^{11}C]butyrate as the potential ligand for positron emission tomography. *J Nucl Med* 1993;34:431–439.
34. Ishitoya J, Yamakawa A, Takenawa T. Translocation of diacylglycerol kinase in response to chemitactic peptide and phorbol ester in neutrophils. *Biochem Biophys Res Commun* 1987;144:1025–1030.
35. Cook S, Palmer S, Wakelam MJO. In: *sn-1,2-Diacylglycerol (DAG) assay reagents system manual.* Code RPN 200. Amersham UK.
36. Davies P, Maloney AJF. Selective loss of central cholinergic neurons in Alzheimer's disease. *Lancet* 1976;2:1403.
37. Whitehouse PJ, Price DL, Struble RG, et al. Alzheimer's disease and senile dementia: loss of neurons in the basal forebrain. *Science* 1982;215:1237–1239.